LANGMUIR
Article
Cite This: *Langmuir* 2018, 34, 14511−14518
pubs.acs.org/Langmuir

Liquid Combination with High Refractive Index Contrast and Fast Scanning Speeds for Electrowetting Adaptive Optics

Wei Yang Lim,[†] Omkar D. Supekar,[†] Mo Zohrabi,[‡] Juliet T. Gopinath,[‡,§] and Victor M. Bright[†]

[†]Department of Mechanical Engineering, [‡]Department of Electrical, Computer, and Energy Engineering and [§]Department of Physics, University of Colorado, Boulder, Colorado 80309, United States

Supporting Information

ABSTRACT: Electrowetting adaptive optical devices are versatile, with applications ranging from microscopy to remote sensing. The choice of liquids in these devices governs its tuning range, temporal response, and wavelength of operation. We characterized a liquid system, consisting of 1-phenyl-1-cyclohexene and deionized water, using both lens and prism devices. The liquids have a large contact angle tuning range, from 173 to 60°. Measured maximum scanning angle was realized at ±13.7° in a two-electrode prism, with simulation predictions of ±18.2°. The liquid's switching time to reach 90° contact angle from rest, in a 4 mm diameter device, was measured at 100 ms. Steady-state scanning with a two-electrode prism showed linear and consistent scan angles of ±4.8° for a 20 V differential between the two electrodes, whereas beam scanning using the liquid system achieved ±1.74° at 500 Hz for a voltage differential of 80 V.

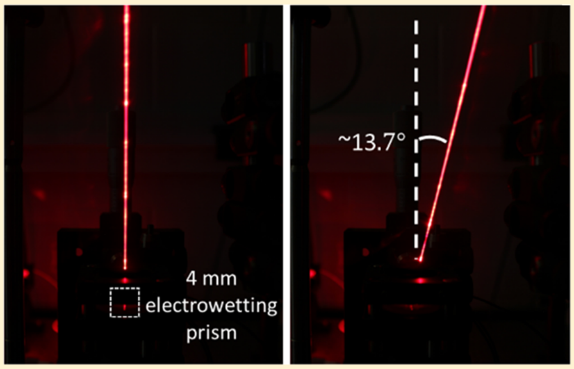

■ INTRODUCTION

The electrowetting on dielectric (EWOD) principle enables the control of the shape of a liquid droplet or a liquid−liquid interface on a dielectric surface through an applied voltage.[1] The result is an ultrasmooth, tunable liquid interface that is an ideal platform for adaptive optics.[2−7] Devices based on the EWOD principle are appealing due to their low power consumption, large range of tunability, transmissive nature, and operation without mechanical moving parts. Typically, two immiscible liquids (polar and nonpolar) that are density matched with contrasting refractive indices are used. These liquids are placed in a glass cylinder or on a planar substrate that is functionalized with an electrode, dielectric, and a hydrophobic coating and attached to a separate ground electrode. In this implementation with a single sidewall electrode in a cylindrical geometry[8−10] or a single concentric electrode for planar geometry,[11−14] the device acts as a variable focus lens. Using two sidewall electrodes enable the operation as a one-dimensional prism, still complete with focusing capabilities.[4,15] Custom liquid interfaces can be achieved by extending to four or more electrodes and used for correcting optical wavefront aberrations.[7,16,17] In all cases, the refractive index contrast between the polar and nonpolar liquids is crucial in determining the lens focal length tunability, prism steering angle, and the extent of aberration correction capability. In addition, the viscosity of the liquids, dependent on both the size of the device and physical properties of the liquid combination, has a large impact on the temporal response.[18]

The concept of using electrowetting-based devices in applications, such as microscopy,[15,19] light detection and ranging (LIDAR),[20] electrowetting displays,[21−23] has been demonstrated recently. The performance for these applications hinges upon both the beam steering capability and the temporal response being comparable to available market systems. For most of the current EWOD prism designs, scanning angles reported are below ±10° with an estimated switching response[24] above 15 ms for millimeter-sized devices. An electrowetting prism by Kopp et al.[6] achieved ±6.4° with 400 ms switching time (5 mm device), Clement et al.[3] demonstrated ±8.8°, whereas Smith et al.[4] measured ±7°. Other works have investigated methods on improving the optical and temporal performance of the liquids used. One of the earliest studies, was performed by Kuiper and Hendriks, which showed that the temporal response of a high refractive index contrast liquids ($\Delta n = 0.17$) can be optimized by tuning the liquid viscosity for critical damping.[8] A method for preparing one of the highest refractive index nonpolar liquids ($n = 1.632$) with low viscosity has also been suggested.[25] Alternatively, liquid studies have explored utilizing fluids aside from water as the polar liquid,[26,27] opening up new liquid combinations for viscosity matching to improve temporal response.[28−30] Here, we demonstrate the implementation of a liquid combination in an EWOD prism, which has a measured maximum scan angle range of ±13.7°. It is important to

Received: August 21, 2018
Revised: October 16, 2018
Published: November 9, 2018

DOI: 10.1021/acs.langmuir.8b02849
Langmuir 2018, 34, 14511−14518

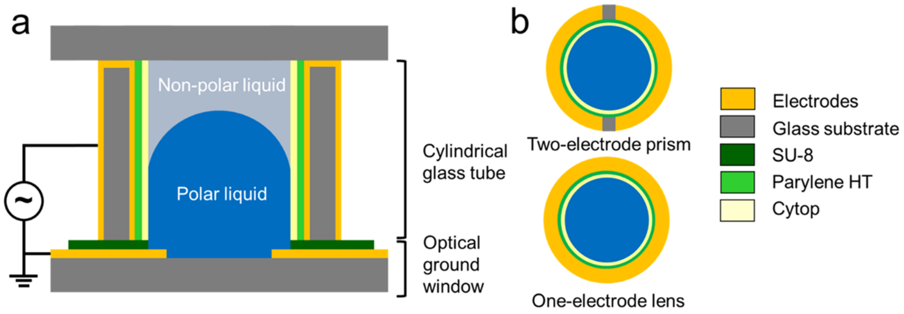

Figure 1. (a) Cross-sectional view of an assembled electrowetting device. The cylindrical glass tube and optical ground window were fabricated separately before being bonded together with an ultraviolet (UV) curable epoxy. (b) Top view of cylindrical glass tube. (Top) Two-electrode prism with vertical side electrodes separated by 400 μm. This was fabricated with a shadow masking technique. (Bottom) Annular electrode enables the uniform actuation of the liquid meniscus as an optical lens.

delineate the switching speed (time to actuate the device from rest) from the achievable scanning speed of an electrowetting prism (time needed to complete a single sweep scan). Our EWOD prism achieved a switching time of 100 ms, while reaching a scanning frequency of 500 Hz with a scan angle of ±1.74°. Both the high scan angle and scanning speed attest to its suitability in LIDAR and microscopy applications.

In this work, we selected a pair of immiscible liquids, with a high refractive index contrast ($\Delta n > 0.2$), low density mismatch (<0.01 g/L), and low viscosities. Although these properties can be optimized by mixing several liquids,[28] to simplify the system, we focused only on pure liquids. Density matching between the two liquids is imperative to the operation of the device irrespective of orientation, by minimizing gravitational distortion. We optimized the refractive index contrast between the polar and nonpolar liquids by examining the theoretical and physical limits. The refractive index of a liquid is directly related to its polarizability through the Lorentz−Lorenz equation. A liquid of low refractive index ($n \sim 1.3$) will therefore require a molecular structure with minimal dipole moment per unit volume.[31] At the lowest refractive index limit, molecules will escape intermolecular attractive forces and transition into a gas phase, whereas at the opposing end of the spectrum, attractive forces are strong enough to solidify the liquid.[32] Because the attractive forces are weakly related to the molecular dipoles, a high density should not be correlated to a high refractive index.[32] Past studies predict the lowest theoretical refractive index organic polymer to be between 1.26 and 1.29. This polymer was constructed from the dipole moment of the individual molecular group.[31] Under standard atmospheric conditions, one of the lowest refractive index materials is Teflon, with a refractive index between 1.29 and 1.31.[31] Another choice is water ($n = 1.33$), close to the experimentally measured lower limit. Water's other physical properties are also attractive and include low mutual solubility with the nonpolar phase,[33] intrinsic conductivity,[27] low toxicity, and high surface tension (72.2 mN/m). These characteristics make it an excellent choice as the polar liquid for our study. Thus, to exceed the specified refractive index contrast, we required the nonpolar liquid to have a refractive index >1.53. Suitable liquid choices include those with phenyl or halogenated molecular groups, which have a larger dipole moment per volume, compared to pure carbon chain liquids.[31] Most of the suitable nonpolar liquids have densities substantially higher than water, which require mixing with an additional liquid to achieve density matching with water.

We examined a large number of liquids based on their physical properties, before selecting the combination of deionized water (DI) and 1-phenyl-1-cyclohexene (PCH). PCH is commercially available and has a refractive index of 1.57 at a wavelength of 589 nm,[34] a density of 0.994 g/L, and a measured viscosity of 3.26 mPa s. Density mismatch between the two liquids system was calculated to be $\Delta\rho = 0.004$ g/L and initial contact angle measurements showed 173° on a hydrophobic surface (Cytop). We characterized the scanning and temporal behaviors of this high refractive index contrast and density-matched liquid combination. First, the contact angle vs driving voltage and the switching time of this liquid combination were measured in a single-electrode electrowetting device. Next, we analyzed beam scanning under steady-state and dynamic conditions in a two-electrode electrowetting prism device. Finally, we demonstrated that the liquid oscillates with scanning frequencies up to 500 Hz with a scan angle of ±1.74°.

■ DEVICE FABRICATION

The fabrication of the one or two-electrode electrowetting devices uses two components, a cylindrical glass tube with patterned vertical electrodes and an optical window with the ground electrode (Figure 1).[35−37] The cylindrical glass tube was made of borosilicate glass, with a 3.95 mm inner diameter and a height of 5 mm. A three-dimensional (3D) printed shadow mask was inserted into the cylindrical glass tube to create a 400 μm electrode separation for the two-electrode electrowetting device. The electrode separation thickness was limited by the lateral resolution of our 3D printed shadow mask. Indium tin oxide (ITO), used as the vertical side electrode, was deposited uniformly along the inner and outer sidewalls of the tube using direct current sputtering at 120 W and an argon pressure of 8 mTorr. The shadow mask was removed, and the conductivity of the ITO vertical electrodes was increased by annealing at 300 °C. Kapton tape was used to mask the outer walls of the tube for electrical connections before the dielectric and hydrophobic layers were applied. A 3 μm layer of Parylene HT (Specialty Coating Systems) was vapor-phase deposited on the inner wall of the glass tube. Finally, the inner wall of the device was dip-coated in a 3% wt hydrophobic Cytop solution and cured at 185 °C for 30 min. A borosilicate glass with annular patterned electrodes was used as the optical ground window. It was first lithographically patterned with NR-7 photoresist. The ground electrode, 50 nm Ti/300 nm Au/50 nm Ti, was evaporated onto the patterned wafer, and the excess metal was removed with a lift-

DOI: 10.1021/acs.langmuir.8b02849
Langmuir 2018, 34, 14511−14518

off process in an acetone bath. SU-8 3050 (50 μm) was deposited and lithographically patterned to serve as an additional dielectric layer between the vertical electrodes and ground electrode.

Next, the Kapton tape and the excess hydrophobic coating on the bottom were removed using a razor blade for better adhesion. The ground electrode and the glass tube were epoxy bonded with a UV curable epoxy (Norland UVS-91). A custom-made printed circuit board (PCB) facilitated electrical access to the two electrodes. The connections between the electrodes and the PCB were formed with a two-part silver epoxy (MG Chemicals 8331-14G) (Figure 2). After assembly, the inner cavity was flushed with isopropanol and deionized water (DI), before blow-drying with air. The final device was filled using a micropipette with 35 μL of DI water and 35 μL of 95% 1-phenyl-1-cyclohexane (PCH), obtained from Sigma-Aldrich. An excess of PCH was used to force out all of the air in between the capping window and the electrowetting device, which prevented the entrapment of air bubbles on the edge of the device.

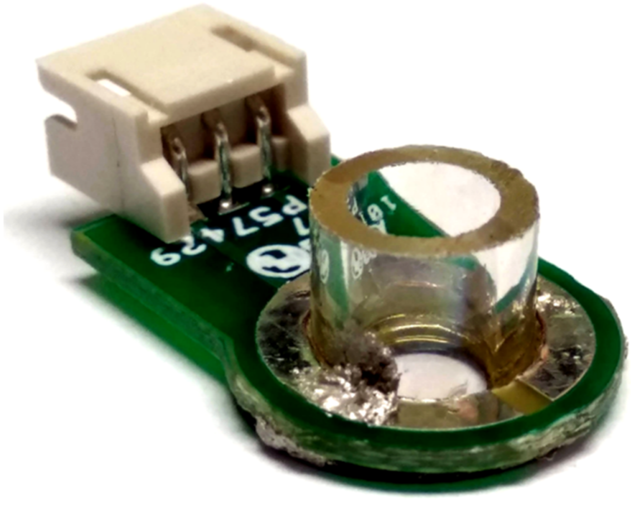

Figure 2. Assembled 4 mm two-electrode electrowetting prism. Indium tin oxide (ITO, 300 nm), as the vertical electrode, was coated on inner and outer sidewalls of the cylindrical tube. The inner wall of the tube was electrically separated by 3 μm Parylene HT and a hydrophobic layer of Cytop. Electrical connections to the device were made through a PCB, bonded to the vertical and ground electrodes with silver epoxy.

EXPERIMENTAL SETUP

A single-electrode lens was used to study the contact angle behavior and switching time of the liquid, whereas a two-electrode prism device was used to investigate the steady-state scan range and dynamic scan response (Figure 3). In both setups, the EWOD device was mounted and centered onto the optical setup using a cage mount system. An optical window was lowered onto the cylinder, sealing the device to prevent evaporation under prolonged testing times. Once the device was fully secured to the cage mount, the excess PCH was carefully wicked off. A continuous wave laser (785 nm) with a 1.2 mm beam diameter (full width half maximum) was spatially filtered and collimated before passing through the optical axis of the device. Without applied voltage, the device acts as diverging lens, and the laser intensity was measured on the photodetector, (Thorlabs DET36A, 70 MHz temporal bandwidth) as a function of applied voltage and frequency. A pinhole (400 μm) positioned directly in front of the photodetector was used as a spatial filter. A sinusoidal input voltage to drive the device was first generated with an analog output data acquisition card (DAQ, National Instruments PCIe-6738) and next amplified (Krohn-Hite Model 7602 Wideband) to the final value. The device was actuated with alternating current (AC) electric fields, with a carrier frequency of 3 kHz. At this frequency, it was experimentally observed that the liquid remains invariant to the instantaneous change in voltage and only responds to the root-mean-square (RMS) value of the applied voltage. Actuation voltages throughout this study are listed as the RMS values.

Contact angle measurements were performed by imaging the liquids through the sidewall of a single-electrode device with a CMOS camera (Chameleon CM3-U3-13Y3M-CS). Captured images were processed using MATLAB, and the contact angles were calculated based on the change in positional height of the liquid meniscus. Minute changes to liquid meniscus curvature will affect the divergence

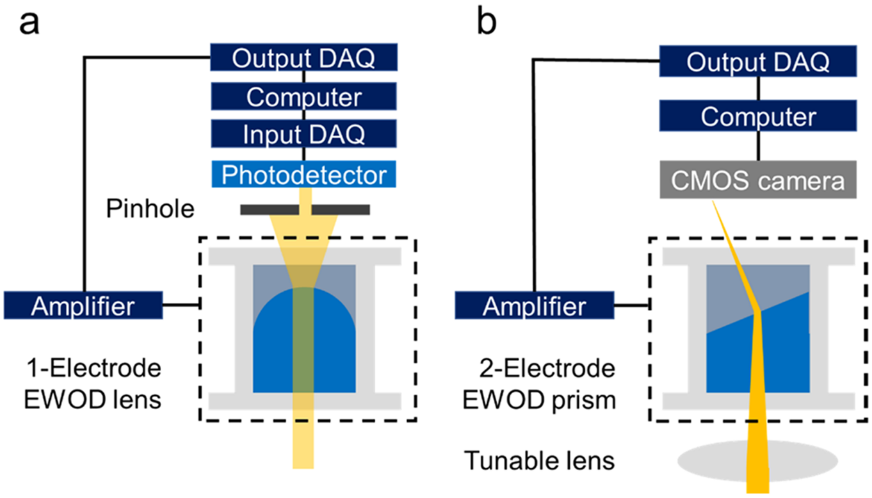

Figure 3. EWOD device driven by a voltage function generated through an amplifier and an analog output data acquisition (DAQ). (a) Experimental setup for contact angle and switching time measurements. Signal from the photodetector passing through a 400 μm pinhole was collected usingan input DAQ, as a measure of the dynamic response at the liquid interface. Contact angle measurements were calculated based off of the liquids meniscus height imaged through the side of the cylindrical tube. (b) Experimental setup for beam steering measurement. The collimated beam was passed through a two-electrode device and focused onto a CMOS camera using a variable focal length lens. Differential voltage applied to the electrodes tilts the meniscus to steer the beam.

of the laser beam passing through. This effect was used to measure the time-dependent dynamics at the liquid−liquid interface as intensity variations on the photodetector (Figure 3a). The output voltage from the photodetector was recorded by an input data acquisition card (MCC-USB-201) connected to a computer. Since other studies[16,35,38] have shown millisecond time scale for liquid dynamics, a sampling rate of 10 kS/s was chosen for the acquisition.

The setup to measure the scanning characteristics of a two-electrode EWOD device (tunable prism) is similar to the technique described, with two key differences. The photodetector was replaced by a CMOS camera, and a variable focus lens, based on a pressure-driven elastic membrane (Optotune EL-10-30), was placed before the tunable prism. This is used for simplicity, instead of a stock lens, to adjust the focused spot on the camera sensor (see Figure 3b). The camera was positioned 21 mm from the meniscus to enable the use of the entire camera sensor area. For steady-state and dynamic measurements, an image of the laser spot was acquired, and scan angles were calculated based on the positional shift. Due to frame rate limitations (150 fps) of the CMOS camera, under dynamic actuation, the camera was replaced with a photodetector with a 400 μm pinhole to detect the oscillation frequency. The intensity spikes from the beam sweeping across the pinhole were analyzed through Fourier analysis.

■ RESULTS AND DISCUSSION

Single-Electrode Characterization. *Contact Angle.* The cylindrical distortion from the wall of the glass tube prevents an accurate measurement of the contact angles directly from an image of the vertical sidewall. Instead, the contact angle was calculated by measuring the meniscus height positioned at the center with the least amount of cylindrical distortion, parallel to the CMOS camera. Since the Bond number (2.528×10^{-5}), a dimensionless ratio of gravitational forces to surface tension, is much less than unity, the curvature of the meniscus was treated as a spherical surface. Its radius can be calculated through the difference between the height at each voltage intervals to the meniscus height at a contact angle of 90°. The contact angle is derived from the radius and geometrical dimensions of the device. Figure 4a−c shows contact angle measurement images taken with the CMOS camera, which were processed using MATLAB before calculating the contact angle. The detected meniscus height was cross-checked with the original image to prevent false detection.

The single-electrode electrowetting device was actuated with a voltage of 0−170 V at intervals of 5 V. The liquid meniscus was given 2 s after each voltage step to reach an equilibrium state before the image was captured. Shown in Figure 4d is the mean contact angle for each device repeated for at least five cycles. The initial contact angle was measured to be 173°. The contact angle of the liquids reduces with increasing applied voltage, as predicted by the Lippmann−Young's equation. At ~95 V, the curve starts deviating from the parabolic behavior, indicating the onset of contact angle saturation. The contact angle curve then follows a linear trend up to 170 V, before reaching complete contact angle saturation[39,40] of 55° at ~200 V. The contact angle at this point is completely invariant to increasing voltages. The standard deviation across the entire range of voltages on each device was calculated to be 1.39°, and deviation between the three devices was 2.59°. Error in the measurements is due to: (1) uncertainty in the meniscus height during curvature inversion and (2) contact angle hysteresis due to surface roughness.[1] The variance seen across the three devices can be attributed to dielectric thickness variations on the device sidewall.

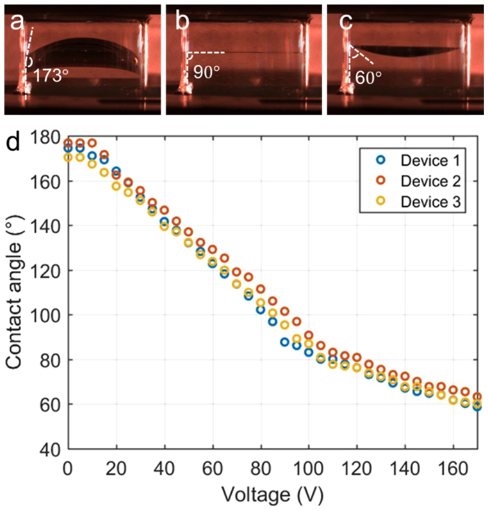

Figure 4. Single-electrode lens with the PCH on the top and DI water on the bottom. The device was actuated using a 3 kHz sinusoidal AC voltage at (a) 0 V_{rms}, (b) 95 V_{rms}, (c) 170 V_{rms}. (d) Mean contact angle of a DI-PCH liquid system measured on three different electrowetting lens, showing contact angle tuning range of 173−60°. Each data point represents the mean contact angle across five cycles. The standard deviation across the five cycles was measured at 1.39°, whereas the deviation across three different devices was 2.59°.

Electrowetting devices often use polar liquids with added surfactants and salts to reduce the voltage requirements of devices by reducing the liquid−liquid interfacial surface tension.[1] To delineate the characteristics of PCH from the effects of ionic charge injection, we avoided the use of additional ions and maintained the resistivity of the DI water at 18 MΩ/cm. Surfactants were not employed, to maintain the liquid's original interfacial surface tension at 24.83 mN/m (this was calculated by fitting the Lippmann−Young equation to the contact angle curve before 95 V and assuming the Cytop thickness to be ~600 nm). This enabled the initial contact angle to reach 173°, allowing a large range of contact angle tuning. Although the interfacial surface tension raises the actuation voltages, the dielectric thickness was chosen such that the voltage applied remained far below the dielectric breakdown strength of Cytop (90 kV/mm) and Parylene HT (212 kV/mm). Repeated cycling of the device (~5000 times) between 0 and 170 V showed that initial contact angles remained within the standard deviation of our initial measurements, further confirming that no permanent charge injection occurred within this voltage range. Despite the lack of external ions, it is well known that DI water can self-ionize[41] and under electric fields partially dissociate into H_3O^+ and OH^- ions.[42,43] Upon actuating the device beyond 200 V, the initial contact angle after multiple cycles was permanently decreased. A previous study has simulated the liquid meniscus near saturation voltages and found that the low contact angle created a wedge-like geometry.[44] This develops a localized electric field strength, much higher than what is experienced by the bulk liquid. Under the intense electric forces, ionic charges in the liquid are pulled toward the dielectric layer, with some being trapped within the dielectric.[45−47] The resulting electrostatic field from the trapped charges screens the applied electric field, reducing the electrowetting effect. To avoid this undesirable effect, we limited the maximum applied voltage to be less than 170 V.

DOI: 10.1021/acs.langmuir.8b02849
Langmuir 2018, 34, 14511−14518

Liquid Switching Time. A photodetector with a pinhole was used to capture the actuation response by measuring the intensity of the beam passing through a single-electrode lens device. The device was actuated from 173 to 90° contact angle, using a step voltage function. When the contact angle was actuated beyond 90° using a step voltage function, in some cases a liquid water droplet detached from the center bulk of the liquid (Figure S1). Due to the close densities of the liquids ($\Delta\rho$ = 0.004 g/L), in our 4 mm diameter devices, gravity effects are negligible, and the ejected droplet remained separated just above the liquid meniscus. As soon as the voltage is turned off, the meniscus reverts to its original curvature ejecting the liquid droplet further into the bulk of the PCH liquid. One possible explanation is that the abrupt change in curvature overcomes interfacial surface tension, causing a water droplet to break off. An analogous case has been observed with liquid droplet detachment from a planar surface, when the electrical energy exceeded the surface energy of adhesion.[48] For high-speed actuation, this instability imposes an experimental limit on the speed of the actuation.

Another factor when determining the switching time of the device, from rest state, is the generation of a standing wave, which propagates along the liquid−liquid meniscus.[35] These oscillations along the meniscus result in intensity oscillations that are recorded on the photodetector. Illustrated in Figure 5, the liquid system reached 2.5% of the final steady-state value within 100 ms. The test was repeated twice with results within 2 ms of each other. Without custom voltage shaping,[35] the response time is limited by viscosity of the liquids and device dimensions.[8,28,29] Intensity oscillations of DI-PCH system displayed similar characteristics to an underdamped system. Actuation within the overdamped regime can reduce the amplitude of the initial standing wave at the expense of device response speed. Ideally, the device should be driven in the critically damped regime by choosing the viscosity of the liquids for the given geometrical dimensions of the lens.[8,30] At the same time, the reduced oscillations along the meniscus may alleviate the issue of liquid droplet ejection.

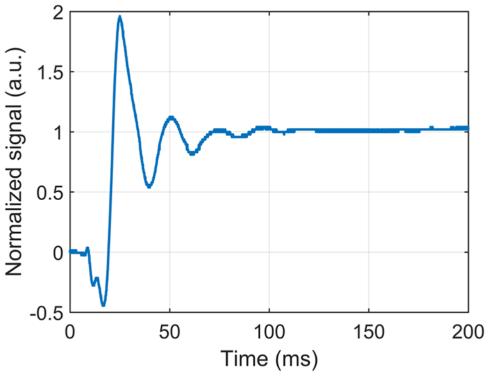

Figure 5. Switching time of DI-PCH in a single-electrode device when actuated from 173 to 90°. Dynamics of liquid oscillation captured by measuring the variations in beam intensity passing through the single-electrode EWOD device on a photodetector. Oscillations dampen out to 2.5% of the final steady-state value within 100 ms.

Two-Electrode Device Characterization. *Beam Steering.* A differential voltage applied to a two-electrode electrowetting prism will cause the meniscus to tilt and steer the optical beam. In the simplest case, where one electrode is kept at ground and the other is kept at a set voltage, the meniscus will tilt with a curvature. This curvature creates additional distortion in the optical beam. An alternative actuation method involves scanning around the ~flat meniscus (contact angle of 90°), reducing the amount of distortion through a more symmetric actuation on the two sides. For example, a device, which requires 95 V to reach a contact angle of 90°, can be driven as a prism by actuating the left electrode to 85 V, and whereas the other to 105 V.

We defined the voltage differential as the difference between the left and right electrodes ($V_{\mathrm{left}} - V_{\mathrm{right}}$). The two-electrode prism was actuated around 95 V at 1 V steps increments to a maximum of 20 V differential. Similar to the contact angle characterization, the CMOS camera captured an image once the liquids reach steady-state after each voltage step. An image of the beam spot is then projected onto x−y axis and fitted with a Gaussian distribution to locate the beam centroid. Using the distance between the liquid meniscus to the CMOS sensor, the steering angle was calculated based on the distance the beam deviated. Figure 6 shows the mean-measured steering angle by actuating the device over the full ranges of voltage for five cycles and the corresponding tilt angles of the meniscus at the maximum voltage differential. The actuation displayed consistent steering angles, reaching a maximum of ±4.8° with an average 0.01° standard deviation. At lower voltage differentials, the actuation was linear with a slight asymmetry between the left and the right actuation due to optical alignment errors. Near differentials of 20 V, additional curvature was induced on the liquid meniscus at the edge of the device. By increasing the number of electrodes in a device,[6] the contact angle at each point around the circumference can be better controlled for a more planar interface.

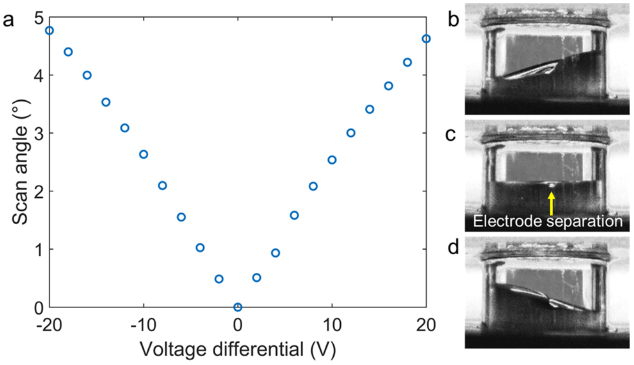

Figure 6. (a) Scanning of a two-electrode prism by tilting the meniscus around the 90° contact angle at 95 V to minimize interface curvature. An image of the beam spot was captured once the liquid reached steady-state after each voltage step. Beam centroid was measured by fitting a Gaussian distribution to the x−y intensity projections and the contact angle was calculated. The voltage differential is defined as ($V_{\mathrm{left}} - V_{\mathrm{right}}$) applied symmetrically around the voltage of 95 V. The standard deviation over the course of five cycles is 0.01°. (Right) Side image of the liquid meniscus at (b) −20 V, (c) 0 V, and (d) 20 V voltage differential with a slight induced curvature. The separation of electrodes (400 μm) can be observed at the center of the device causing a minor curvature.

To reach larger scan ranges, we drove the device at 100 V differential around the flat voltage of 100 V. The maximum steering angle was measured to be ±13.7 with a standard deviation of ±0.5°. Beyond 100 V differential, the tilt angle exceeds the vertical height of the sealed device and contacts

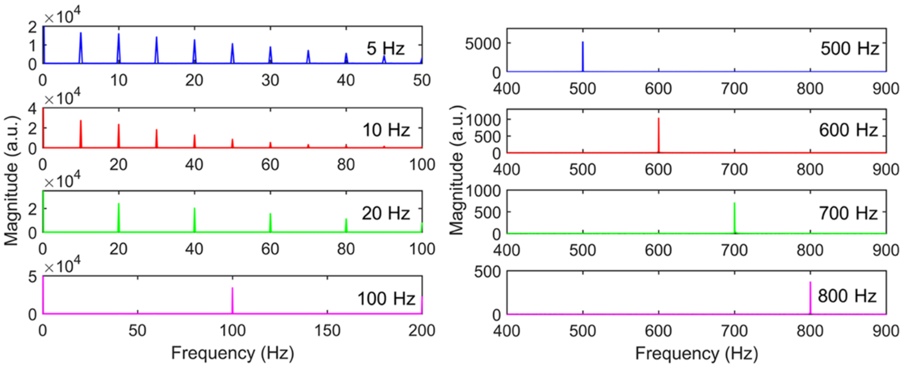

Figure 7. Beam scanning speeds by modulating the input voltage function at set sweeping frequencies with a voltage differential of 20 V. Photodetector intensity oscillations, with input sweeping frequencies of 5, 10, 20, 100, 500, 600, 700, and 800 Hz over a period of 10 s, were collected and analyzed through Fourier transforms.

the top boundary window. To investigate the steering limits of our device, the liquid−liquid interface was simulated in MATLAB, by solving the Young−Laplace equation.[17,49] The contact angles were chosen to match experimental conditions with 65° on one electrode and 125° on the other. The resulting surface was imported into Zemax as a grid sag surface, and the maximum scanning angle was evaluated to be ±18.2°. Simulation results showed that the liquid surface reached the top and lower boundary of the device (5 mm), whereas the experimentally measured tilt reached a height of 4.2 mm. The discrepancy between the predicted and measured values could thus be attributed to the slight offset of the meniscus from the center of the device. Additionally, it is difficult to achieve the predicted maximum scanning angle because minute vibrations along the liquid meniscus can force the liquid into contact with the upper and lower boundaries. Interestingly, the simulation showed that the curvature induced from the liquid interface increased the scanning angle, at the center of the liquid meniscus, when compared to a planar surface of a similar tilt.

Scanning Speed. For beam scanning, the driving input voltage function was modulated at a set sweep frequency. The scan was performed around the 90° contact angle. Voltages on the two electrodes are cycled between 85 and 105 V_{rms} (generating a 20 V differential at peak) with a phase delay of 180°. This would correspond to a contact angle of 100 and 80° on each electrode, which will tilt the meniscus similarly to Figure 6. The similar 3 kHz sinusoidal carrier wave was superimposed onto the sweeping voltage function. The sweep frequency was kept sufficiently below the carrier wave frequency to avoid aliasing of the two frequencies. It is necessary for the driving voltage function to oscillate between positive and negative potentials to prevent contact angle relaxation, in which actuated contact angle slowly drops from its actuated state over milliseconds to seconds. Current hypothesis suggests that contact angle relaxation occurs when the nonzero dipole moment of the molecules reacts to the low-frequency electric fields.[21] This has been seen in studies of high refractive index liquids due to the highly polarized molecular groups.[21,25]

A photodetector positioned on the optical axis was used to characterize the liquid oscillatory frequency response, whereas the CMOS camera was used to estimate the maximum scan angle at the specified frequency. Intensity measurements from the photodetector were analyzed using Fourier analysis (Figure 7). The fundamental frequency measured show excellent correlation with input sweeping frequencies up to 800 Hz. Subsequent intensity peaks in the Fourier analysis indicate additional modes of the fundamental frequency. Measured scanning angles decreased dramatically after the sweeping frequency exceeded 1 Hz (Figure 8). At a sweep frequency of 10 Hz, the scan angle range dropped from ±4.8° at 1 Hz to ±2.86°, with only ±0.47° was measured at 500 Hz. Intensity oscillations at 800 Hz could still be recorded using a photodetector, but the scan range became too small to resolve on the CMOS camera. Even at increased voltage differential, the phenomenon of liquid droplet ejection has not been observed throughout the scanning experiments. Unlike the switching response, the liquid contact line was driven with a sinusoidal voltage function resulting in the tilt angles to vary gradually. This, in combination with the dramatically reduced amplitude at higher frequencies, ensured that the induced oscillations were not large enough to overcome the liquid surface tension.

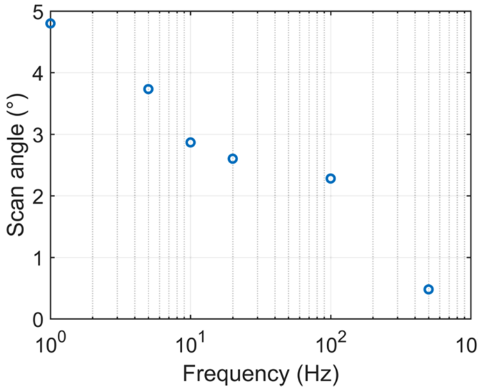

Figure 8. Mean maximum scan angles over five cycles, with 20 V voltage differential at frequencies of 1, 5, 10, 20, 100, and 500 Hz were recorded on a CMOS camera. Oscillations beyond 800 Hz had scan angles smaller than the beam spot size, making it difficult for the CMOS camera to resolve. The total scan range is twice the scan angle. Standard deviation of measured scan angles was less than 0.1°.

Comparing the maximum scan angle obtained in dynamic scanning to steady state, at 1 Hz, both methods yielded consistent results at ± 4.8° with a 20 V differential. The scan range decreases after 1 Hz can be attributed to the frequency response of the liquids in the given device geometry, whereby the scanning frequency exceeded the time needed for the liquids to fully respond to the applied voltage, hence

DOI: 10.1021/acs.langmuir.8b02849
Langmuir 2018, 34, 14511−14518

interrupting the motion of the liquids. This behavior is common with dynamic systems actuated beyond their roll-off frequency. Studies have shown that microscale-sized liquid droplets oscillate in response to forcing functions with 100+ Hz frequencies.[50,51] The scanning frequency limit can thus be extended in part by applying a higher voltage differential, which increases electromechanical force on the triple contact line, accelerating liquid motion. When the voltage differential of 80 V is applied at 500 Hz, the scan angle was increased to ±1.74°. Alternatively, the small scanning angles at higher frequency can be improved by magnification through optical designs or using a higher refractive index contrast liquid.

CONCLUSIONS

In summary, we have demonstrated a density-matched liquid combination of DI-PCH, suitable for electrowetting, with excellent characteristics. Steady-state scanning of a two-electrode prism up to ±4.8° exhibited linear and reliable scan angles. The high refractive index contrast of 1.57−1.33 and tuning range (173−60°) of the liquid system enabled experimentally measured beam scanning angle of ±13.7°, which is only limited by the geometry of our device and amount of respective liquids filled in the device. Simulation results with perfectly equal amounts of liquids in the device geometry predicted up to ±18.2° degree of scanning. Liquid switching time, actuated from 173 to 90°, was measured to be 100 ms. We experimentally showed that under dynamic operation, in a 4 mm diameter electrowetting device, the liquids respond to sweep frequencies of up to 800 Hz. After 1 Hz, the scan angle decreased dramatically as the liquid motion is interrupted by the voltage function before completing the entire oscillation. At 500 Hz, scan angle of ±0.47° at 20 V differential was measured, which was increased to ±1.74° with an 80 V differential between the two electrodes. The combination of high refractive index contrast and fast scanning speeds shows that DI-PCH liquid system is suitable for high-performance applications, such as microscopy, LIDAR, and imaging.

ASSOCIATED CONTENT

Supporting Information

The Supporting Information is available free of charge on the ACS Publications website at DOI: 10.1021/acs.langmuir.8b02849.

Liquid droplet ejection of deionized water and 1-phenyl-1-cyclohexene (PDF)

AUTHOR INFORMATION

ORCID

Wei Yang Lim: 0000-0002-6954-3199
Omkar D. Supekar: 0000-0003-1777-8508

Funding

This work was supported by the National Science Foundation (NSF) (IDBR) DBI-1353757 and (NCS_FO) CBET-1631704, the National Institutes of Health (NIH) (SPARC) 1OT2OD023852 and (BRAIN) U01 NS099577-02 and the Office of Naval Research (ONR) N00014-15-1-2739.

Notes

The authors declare no competing financial interest.

ACKNOWLEDGMENTS

The authors would like to thank Parag Shah from the University of Colorado Boulder for measuring the viscosity of PCH.

REFERENCES

(1) Mugele, F.; Baret, J.-C. Electrowetting: From Basics to Applications. *J. Phys.: Condens. Matter* **2005**, *17*, R705−R774.

(2) Li, L.; Liu, C.; Ren, H.; Deng, H.; Wang, Q.-H. Annular Folded Electrowetting Liquid Lens. *Opt. Lett.* **2015**, *40*, 1968−1971.

(3) Clement, C. E.; Thio, S. K.; Park, S. Y. An Optofluidic Tunable Fresnel Lens for Spatial Focal Control Based on Electrowetting-on-Dielectric (EWOD). *Sens. Actuators, B* **2017**, *240*, 909−915.

(4) Smith, N. R.; Abeysinghe, D. C.; Haus, J. W.; Heikenfeld, J. Agile Wide-Angle Beam Steering with Electrowetting Microprisms. *Opt. Express* **2006**, *14*, 6557.

(5) Lee, J. S.; Jung, G. S.; Won, Y. H. In *Light Field 3D Endoscope Based on Electro-Wetting Lens Array*, Proceedings SPIE 10061, Microfluidics, BioMEMS, and Medical Microsystems XV, 2017; p 100610J.

(6) Kopp, D.; Lehmann, L.; Zappe, H. Optofluidic Laser Scanner Based on a Rotating Liquid Prism. *Appl. Opt.* **2016**, *55*, 2136.

(7) Lima, N. C.; Mishra, K.; Mugele, F. Aberration Control in Adaptive Optics: A Numerical Study of Arbitrarily Deformable Liquid Lenses. *Opt. Express* **2017**, *25*, 6700.

(8) Kuiper, S.; Hendriks, B. H. W. Variable-Focus Liquid Lens for Miniature Cameras. *Appl. Phys. Lett.* **2004**, *85*, 1128−1130.

(9) Berge, B.; Peseux, J. Variable Focal Lens Controlled by an External Voltage: An Application of Electrowetting. *Eur. Phys. J. E* **2000**, *3*, 159−163.

(10) Murade, C. U.; van der Ende, D.; Mugele, F. High Speed Adaptive Liquid Microlens Array. *Opt. Express* **2012**, *20*, 18180.

(11) Shahini, A.; Jin, H.; Zhou, Z.; Zhao, Y.; Chen, P. Y.; Hua, J.; Cheng, M. M. C. Toward Individually Tunable Compound Eyes with Transparent Graphene Electrode. *Bioinspiration Biomimetics* **2017**, *12*, No. 046002.

(12) An, J. Y.; Hur, J. H.; Kim, S.; Lee, J. H. Spherically Encapsulated Variable Liquid Lens on Coplanar Electrodes. *IEEE Photonics Technol. Lett.* **2011**, *23*, 1703−1705.

(13) Shahini, A.; Zeng, P.; Zhao, Y.; Cheng, M. M. C. In *Individually Tunable Liquid Lens Arrays Using Transparent Graphene for Compound Eye Applications*, IEEE 29th International Conference on Micro Electro Mechanical Systems (MEMS); IEEE, 2016; pp 597−600.

(14) Yi, U. C.; Kim, C. J. Characterization of Electrowetting Actuation on Addressable Single-Side Coplanar Electrodes. *J. Micromech. Microeng.* **2006**, *16*, 2053−2059.

(15) Supekar, O. D.; Ozbay, B. N.; Zohrabi, M.; Nystrom, P. D.; Futia, G. L.; Restrepo, D.; Gibson, E. A.; Gopinath, J. T.; Bright, V. M. Two-Photon Laser Scanning Microscopy with Electrowetting-Based Prism Scanning. *Biomed. Opt. Express* **2017**, *8*, 5412.

(16) Kopp, D.; Zappe, H. Tubular Astigmatism-Tunable Fluidic Lens. *Opt. Lett.* **2016**, *41*, 2735−2738.

(17) Zohrabi, M.; Cormack, R. H.; Mccullough, C.; Supekar, O. D.; Gibson, E. A.; Bright, V. M.; Gopinath, J. T. Numerical Analysis of Wavefront Aberration Correction Using Multielectrode Electrowetting-Based Devices. *Opt. Express* **2017**, *25*, 31451.

(18) Baret, J. C.; Decré, M. M. J.; Mugele, F. Self-Excited Drop Oscillations in Electrowetting. *Langmuir* **2007**, *23*, 5173−5179.

(19) Li, L.; Wang, D.; Liu, C.; Wang, Q.-H. Zoom Microscope Objective Using Electrowetting Lenses. *Opt. Express* **2016**, *24*, 2931.

(20) Zohrabi, M.; Cormack, R. H.; Gopinath, J. T. Wide-Angle Nonmechanical Beam Steering Using Liquid Lenses. *Opt. Express* **2016**, *24*, 23798.

(21) Zhou, K.; Heikenfeld, J.; Dean, K. A.; Howard, E. M.; Johnson, M. R. A Full Description of a Simple and Scalable Fabrication Process for Electrowetting Displays. *J. Micromech. Microeng.* **2009**, *19*, No. 065029.

(22) Murade, C. U.; Oh, J. M.; van den Ende, D.; Mugele, F. Electrowetting Driven Optical Switch and Tunable Aperture. *Opt. Express* **2011**, *19*, 15525.

(23) Li, L.; Liu, C.; Ren, H.; Wang, Q. H. Optical Switchable Electrowetting Lens. *IEEE Photonics Technol. Lett.* **2016**, *28*, 1505−1508.

(24) Smith, N. R.; Hou, L.; Zhang, J.; Heikenfeld, J. In *Experimental Validation of >1 KHz Electrowetting Modulation*, 17th Biennial University/Government/Industry Micro/Nano Symposium, 2008; pp 11−14.

(25) Zhang, J.; Van Meter, D.; Hou, L.; Smith, N.; Yang, J.; Stalcup, A.; Laughlin, R.; Heikenfeld, J. Preparation and Analysis of 1-Chloronaphthalene for Highly Refractive Electrowetting Optics. *Langmuir* **2009**, *25*, 10413−10416.

(26) Chatterjee, D.; Hetayothin, B.; Wheeler, A. R.; King, D. J.; Garrell, R. L. Droplet-Based Microfluidics with Nonaqueous Solvents and Solutions. *Lab Chip* **2006**, *6*, 199−206.

(27) Chevalliot, S.; Heikenfeld, J.; Clapp, L.; Milarcik, A.; Vilner, S. Analysis of Nonaqueous Electrowetting Fluids for Displays. *J. Disp. Technol.* **2011**, *7*, 649−656.

(28) Hong, J.; Kim, Y. K.; Kang, K. H.; Oh, J. M.; Kang, I. S. Effects of Drop Size and Viscosity on Spreading Dynamics in DC Electrowetting. *Langmuir* **2013**, *29*, 9118−9125.

(29) Jung, G. S.; Lee, J. S.; Won, Y. H. In *Effects of Liquid Property and Substrate Roughness on the Response Time of an Electrowetting Liquid Lens*, MOEMS and Miniaturized Systems XVII, 2018; 1054516.

(30) Shahini, A.; Xia, J.; Zhou, Z.; Zhao, Y.; Cheng, M. M. C. Versatile Miniature Tunable Liquid Lenses Using Transparent Graphene Electrodes. *Langmuir* **2016**, *32*, 1658−1665.

(31) Groh, W.; Zimmermann, A. What Is the Lowest Refractive Index of an Organic Polymer? *Macromolecules* **1991**, *24*, 6660−6663.

(32) West, C. D. Immersion Liquids of High Refractive Index. *Am. Mineral.* **1960**, 245−249.

(33) Fedors, R. F. A Method for Estimating Both the Solubility Parameters and Molar Volumes of Liquids. *Polym. Eng. Sci.* **1974**, *14*, 147.

(34) Sigma-Aldrich. 1-Phenyl-1-cyclohexene 95%, 2018. https://www.sigmaaldrich.com/catalog/product/aldrich/p22303?lang=en&region=US&gclid=EAIaIQobChMIjZidxZPw3AIVh0BpCh3FiQd8EAAYASAAEgLDg_D_BwE (accessed Aug 15, 2018).

(35) Supekar, O. D.; Zohrabi, M.; Gopinath, J. T.; Bright, V. M. Enhanced Response Time of Electrowetting Lenses with Shaped Input Voltage Functions. *Langmuir* **2017**, *33*, 4863−4869.

(36) Terrab, S.; Watson, A. M.; Roath, C.; Gopinath, J. T.; Bright, V. M. Adaptive Electrowetting Lens-Prism Element. *Opt. Express* **2015**, *23*, 25838.

(37) Watson, A. M.; Dease, K.; Terrab, S.; Roath, C.; Gopinath, J. T.; Bright, V. M. Focus-Tunable Low-Power Electrowetting Lenses with Thin Parylene Films. *Appl. Opt.* **2015**, *54*, 6224−6229.

(38) Montoya, R. D.; Underwood, K.; Terrab, S.; Watson, A. M.; Bright, V. M.; Gopinath, J. T. Large Extinction Ratio Optical Electrowetting Shutter. *Opt. Express* **2016**, *24*, 9660.

(39) Klarman, D.; Andelman, D.; Urbakh, M. A Model of Electrowetting, Reversed Electrowetting and Contact Angle Saturation. *Langmuir* **2011**, *27*, 6031−6041.

(40) Chevalliot, S.; Kuiper, S.; Heikenfeld, J. Experimental Validation of the Invariance of Electrowetting Contact Angle Saturation. *J. Adhes. Sci. Technol.* **2012**, *26*, 1909−1930.

(41) Eigen, M.; de Maeyer, L. Self-Dissociation and Protonic Charge Transport in Water and Ice. *Proc. R. Soc. A* **1958**, *247*, 505−533.

(42) Geissler, P. L.; Dellago, C.; Chandler, D.; Hutter, J.; Parrinello, M. Autoionization in Liquid Water. *Science* **2001**, *291*, 2121−2124.

(43) Stuve, E. M. Ionization of Water in Interfacial Electric Fields: An Electrochemical View. *Chem. Phys. Lett.* **2012**, *519*−*520*, 1−17.

(44) Drygiannakis, A. I.; Papathanasiou, A. G.; Boudouvis, A. G. On the Connection between Dielectric Breakdown Strength, Trapping of Charge, and Contact Angle Saturation in Electrowetting. *Langmuir* **2009**, *25*, 147−152.

(45) Raj, B.; Dhindsa, M.; Smith, N. R.; Laughlin, R.; Heikenfeld, J. Ion and Liquid Dependent Dielectric Failure in Electrowetting Systems. *Langmuir* **2009**, *25*, 12387−12392.

(46) Kedzierski, J. T.; Batra, R.; Berry, S.; Guha, I.; Abedian, B. Validation of the Trapped Charge Model of Electrowetting Contact Angle Saturation on Lipid Bilayers. *J. Appl. Phys.* **2013**, *114*, No. 024901.

(47) Verheijen, H. J. J.; Prins, M. W. J. Reversible Electrowetting and Trapping of Charge: Model and Experiments. *Langmuir* **1999**, *15*, 6616−6620.

(48) Lee, S. J.; Hong, J.; Kang, K. H.; Kang, I. S.; Lee, S. J. Electrowetting-Induced Droplet Detachment from Hydrophobic Surfaces. *Langmuir* **2014**, *30*, 1805−1811.

(49) Lee, S.-L.; Yang, C.-F. Numerical Simulation for Meniscus Shape and Optical Performance of a MEMS-Based Liquid Micro-Lens. *Opt. Express* **2008**, *16*, 19995−20007.

(50) Hong, J. S.; Ko, S. H.; Kang, K. H.; Kang, I. S. A Numerical Investigation on AC Electrowetting of a Droplet. *Microfluid. Nanofluid.* **2008**, *5*, 263−271.

(51) García-Sánchez, P.; Ramos, A.; Mugele, F. Electrothermally Driven Flows in Ac Electrowetting. *Phys. Rev. E* **2010**, *81*, No. 015303.